A Bernoulli-reproducing kernel method for a class of nonlinear singular boundary value problems

Azam Ghasemi*, Abbas Saadatmandi†
Department of Applied Mathematics, Faculty of Mathematical Sciences, University of Kashan, Kashan 87317-53153, Iran

Abstract: We have developed a highly accurate numerical method called Bernoulli-RKM to solve nonlinear singular boundary value problems (SBVPs). This approach uses Bernoulli polynomials and the traditional reproducing kernel method (RKM) and applies the quasi-linearization method to linearize the SBVPs. We have discussed the error and convergence of Bernoulli-RKM and provided numerical examples to demonstrate its potential in solving nonlinear SBVPs. Additionally, we have compared our results with those in existing literature.

Keywords: singular, boundary value problems, reproducing kernel method, Bernoulli polynomials, quasi-linearization method.
Mathematics Subject Classification: 46E22, 65L60, 34B15

1 Introduction

One significant class of boundary value problems that plays a vital role in technology and science is the nonlinear SBVPs. These problems appear in the modeling of nuclear physics, gas dynamics, chemical reactions, electrohydrodynamics, and many engineering applications (see [1, 2, 3] and references therein). In this work, we consider the following SBVP with nonlinear source function $g(x, \nu(x))$ [4, 5, 6]:

$$\nu''(x) + \frac{\lambda}{x}\nu'(x) = g(x, \nu(x)), \quad x \in (0, 1], \qquad \lambda \geq 1, \tag{1}$$

with Neumann and Robin boundary conditions (NBCs/RBCs):

$$\nu'(0) = 0, \qquad \gamma\nu(1) + \zeta\nu'(1) = \rho, \tag{2}$$

where $\gamma > 0$, $\zeta \geq 0$ and ρ is a real constant. It is assumed that $\frac{\partial g}{\partial \nu} \geq 0$ for each of $x \in (0, 1]$, and $g(x, \nu)$, $\frac{\partial g}{\partial \nu}$ are continuous on $(0, 1]$. The existence and uniqueness of the solutions to problem (1)-(2) are discussed by Pandey and Verma [7]. Problem (1)-(2) for different λ appears in many chemical, physical and biological models. For instance, below is a brief introduction to some types.

(i) Eq. (1) with $\lambda = 2$ and $g(x, \nu) = \dfrac{\sigma\nu}{\nu + \varrho}$, $\sigma > 0$, $\varrho > 0$, occurs during modeling of steady-state oxygen diffusion uptake kinetics [3].

*E-mail address: azamghasemi444@gmail.com
†E-mail address: saadatmandi@kashanu.ac.ir, a.saadatmandi@gmail.com, Corresponding author (A. Saadatmandi),
Tel.: +98 31 55912361; fax: +98 31 55552332.

(ii) Eq. (1) with $\lambda = 2$ and $g(x, \nu) = -\sigma e^{-\mu\nu}$, $\sigma > 0$, $\mu > 0$, occurs during modeling of the distribution of heat source in the human head [2].

(iii) Eq. (1) with $\lambda = 1, 2$ and $g(x, \nu) = \theta e^{\nu}$, ($\theta$ is a physical parameter), occurs in studying the electric double layer in a salt-free solution and the theory of thermal explosions [8].

(iv) Eq. (1) with $\lambda = 0, 1, 2$ and $g(x, \nu) = \varphi^2 \nu^m$, ($\varphi > 0$ and $m \in \mathbb{R}$), occurs in studying the reaction-diffusion process in a porous catalyst [9].

(v) Eq. (1) with $\lambda = 2$ and $g(x, \nu) = -\nu^5$, appears from the study of equilibrium of the isothermal gas sphere [10].

The existence of a singularity at $x = 0$ is one of the difficulties that researchers face when solving problem (1)-(2). There are two classes of methods for solving SBVPs: numerical and analytical. Although most of the analytical techniques provide detailed information about the existence and uniqueness of the solutions, however, some criticisms are inflicted on these techniques. Some advantages and disadvantages of analytical techniques for solving SBVPs can be seen in [11]. Due to existing difficulties in analytical techniques, researchers have explored numerical approaches to solve SBVPs. For instance, an approach based on the Adomian decomposition method and Green's function [12], Sinc-Galerkin method [9], variational iteration method involving Adomian polynomials [13], Quasi-Newton's method and the simplified reproducing kernel method (SRKM) [5], SRKM and least squares method [4], advanced Adomian decomposition method [6], improved differential transform method [14], a technique based on the operational matrix of the derivative of the orthonormal Bernoulli polynomials [15], Cubic spline method [16], modified homotopy analysis method [10], modified homotopy perturbation algorithm [17], domain decomposition optimal homotopy analysis method [18], discrete optimized homotopy analysis method [19], iterative approach based on an improved homotopy analysis method [20], and B-spline collocation method [21], are presented for solving problem (1)-(2). Also, in [22], Liu et al. developed a boundary shape function iterative method, and in [23] Roul et al. employed a finite difference method for solving problem (1)-(2) with source function $g(x, \nu, \nu')$. Among other available numerical methods for solving SBVPs, the spectral poly-sinc collocation technique [24], combination of the differential transform method and the Padé approximations and Chebyshev finite difference method [25], Legendre reproducing kernel method [11], compact finite difference method [26], modified Lucas polynomials derivative operational matrix method [27], a hybrid stochastic numerical solver [1], DE sinc-collocation method [28], a method based on sextic B-spline collocation approach [29], two methods based on quintic B-spline collocation approach [30], and a non-uniform mesh optimal cubic B-spline collocation method [31], can be mentioned. Also, the authors of [32] deal with the spectral problems associated with SBVPs and, Pandey et al. [33] described an analytical method based on the combination of Newton's quasi-linearization method and the Picard iteration method for solving a class of doubly SBVPs. Moreover, for some other useful techniques on this subject we refer the interested reader to a method based on the linear B-spline functions [34], variational iteration method [35], local radial basis functions [36], homotopy analysis method [37], and the Adomian decomposition method [38].

Historically, the idea of reproducing kernels is not new. In 1908, Zaremba introduced this concept while considering harmonic functions [39]. In recent years, there have been many publications on solving different types of problems, including SBVPs, using RKM (see say [4, 5, 11, 40] and references therein). Using the traditional RKM, a lot of time is needed in the Gram-Schmidt orthogonalization process [4]. Furthermore, classical RKM requires selecting a dense set of points to obtain a highly accurate solution [11]. To overcome these disadvantages, some researchers

have applied different techniques to traditional RKM (see for example [11, 41, 42, 43]).
In the present research, we improve the traditional RKM for solving problem (1)-(2). We use the idea of traditional RKM and the properties of Bernoulli polynomials to present a new Bernoulli-RKM. We use the idea of traditional RKM and the properties of Bernoulli polynomials to present a new Bernoulli-RKM. The novelties of this research include:

(i) The new technique introduced in this paper removes the necessity for an orthogonalization procedure, a step that is essential in the traditional RKM.

(ii) The Bernoulli-RKM does not depend on a dense set of points; rather, it employs collocation points. Consequently, we expect the speed and accuracy of Bernoulli-RKM to be improved compared to traditional RKM.

(iii) Other SBVPs can be solved using this approach with certain adjustments.

The remainder of this paper is organized as follows. Section 2 introduces Bernoulli polynomials and shows how to create reproduction kernels in polynomial form. In Section 3, we describe Bernoulli-RKM in full detail to solve problem (1)-(2). Also in this section, we discuss the convergence analysis of the Bernoulli-RKM. In Section 4, several numerical examples are presented and compared with the results of other methods in the literature. Section 5 is related to our conclusion about the Bernoulli-RKM.

2 Orthonormal Bernoulli polynomials and corresponding reproducing kernel space

Here we describe some of the preparations used in this study.

2.1 Orthonormal Bernoulli polynomials

The well-known Bernoulli polynomials $\mathcal{B}_i(x)$, $i = 0, 1, \ldots$ of order i are defined on the unit interval $[0, 1]$ as [44]:

$$\mathcal{B}_i(x) = \sum_{\tau=0}^{i} \binom{i}{\tau} \phi_\tau x^{i-\tau},$$

where ϕ_τ, $(\tau = 0, 1, \ldots, i)$ are Bernoulli numbers, which can be defined by

$$\phi_0 = 1, \qquad \phi_i = -\sum_{\tau=0}^{i-1} \binom{i}{\tau} \frac{\phi_\tau}{i+1-\tau}, \quad i \geq 1.$$

Some properties of these polynomials can be seen in [45]. It is noteworthy that Bernoulli polynomials are not orthogonal. However, the orthonormal Bernoulli polynomials (OBPs) can be obtained using the Gram-Schmidt orthogonalization process. As stated in [45], the analytical form of OBPs on $[0, 1]$ is as follows:

$$\psi_i(x) = \sum_{\tau=0}^{i} \beta_i^\tau x^{i-\tau}, \qquad i = 0, 1, \ldots,$$

where β_i^τ is given as

$$\beta_i^\tau = \sqrt{2i+1}(-1)^\tau \binom{i}{\tau} \binom{2i-\tau}{i-\tau}.$$

These polynomials create an orthonormal basis for $L^2[0,1]$. Note that there are several advantages to approximating functions using Bernoulli polynomials instead of Legendre polynomials [44].

2.2 Using OBPs to create a new reproducing kernel space

We start by introducing some concepts. For a given set X, we consider

$$\mathcal{W} = \{\nu(\xi)|\ \nu(\xi) \text{ is a real-valued or complex function}, \xi \in X\},$$

as a Hilbert space with an inner product

$$\langle \nu(\xi), w(\xi)\rangle_{\mathcal{W}}, \qquad \nu(\xi), w(\xi) \in \mathcal{W}.$$

Definition 2.1. ([40, page 3]). If for each fixed $x \in X$ there exists a function $\mathsf{K}(\xi, x)$, such that $\mathsf{K}(\xi, x) \in \mathcal{W}$ and also $\forall \nu(\xi) \in \mathcal{W}$ we have

$$\langle \nu(\xi), \mathsf{K}(\xi, x)\rangle_{\mathcal{W}} = \nu(x),$$

then $\mathsf{K}(\xi, x)$ is known as the reproducing kernel of $\mathcal{W}$ and $\mathcal{W}$ is known as the reproducing kernel space.

Also, we use $\mathcal{W}^{p_{(n)}}[0,1]$ to represent the inner product space of polynomials of degree $\leq n$ on $[0,1]$. For any $\nu, w \in \mathcal{W}^{p_{(n)}}[0,1]$, we define the inner product and the norm as:

$$\langle \nu, w\rangle_{\mathcal{W}^{p_{(n)}}[0,1]} = \int_0^1 \nu(x) w(x)\, dx, \qquad \|\nu\|_{\mathcal{W}^{p_{(n)}}} = \sqrt{\langle \nu, \nu\rangle_{\mathcal{W}^{p_{(n)}}}},$$

respectively. Since $\mathcal{W}^{p_{(n)}}[0,1]$ is a closed finite-dimensional subspace of $L^2[0,1]$, we know that $\mathcal{W}^{p_{(n)}}[0,1]$ is a $(n+1)$-dimensional Hilbert space [46]. Therefore, we have $\langle \nu, w\rangle_{\mathcal{W}^{p_{(n)}}} = \langle \nu, w\rangle_{L^2}$ and $\|\nu\|_{\mathcal{W}^{p_{(n)}}} = \|\nu\|_{L^2}$. Also, it is clear that $\{\psi_i(x)\}_{i=0}^n$ is an orthonormal basis for $\mathcal{W}^{p_{(n)}}[0,1]$.

Theorem 2.2. $\mathcal{W}^{p_{(n)}}[0,1]$ is a reproducing kernel space and its polynomial reproducing kernel function is

$$\mathcal{K}(\xi, x) = \sum_{i=0}^{n} \psi_i(x)\psi_i(\xi). \tag{3}$$

Proof. See [40, Example 1.1.2]. □

3 Solution of problem (1)-(2) by Bernoulli-RKM

Since Eq. (1) is nonlinear, we first need to linearize this equation. We use the quasi-linearization method (QLM) [33, 47, 48] to change the nonlinear Eq. (1) into a sequence of linear equations. Then we use the Bernoulli-RKM to solve these linear equations at each iteration. Utilizing the QLM to problem (1)-(2) determines the $(k+1)$th iterative approximation ν_{k+1}, $(k = 0, 1, 2, \cdots)$ as a solution of the following linear SBVP:

$$\nu''_{k+1}(x) + \frac{\lambda}{x}\nu'_{k+1}(x) + d_k(x)\nu_{k+1}(x) = b_k(x), \tag{4}$$

$$\nu'_{k+1}(0) = 0, \qquad \gamma\nu_{k+1}(1) + \zeta\nu'_{k+1}(1) = \rho, \tag{5}$$

where $d_k(x) = -g_\nu\big(x, \nu_k\big)$ and $b_k(x) = g\big(x, \nu_k\big) - \nu_k g_\nu\big(x, \nu_k\big)$. Here, $g_\nu = \partial g/\partial\nu$ is the functional derivative of $g\,(x, \nu)$.

Remark 3.1. Mandelzweig et al. [47] formulated and explained the general conditions under which second-order and uniform convergence can be proved in the QLM for solving nth-order nonlinear ordinary differential equations. The predicted trend is that this method produces rapid convergence. In other words, if $\Delta\nu_{k+1}(x) = \nu(x) - \nu_{k+1}(x)$ be the difference between the exact solution of problem (1)-(2) and the $(k+1)$-th iteration in Eq. (4), then $\|\Delta\nu_{k+1}\| \leq \mu\|\Delta\nu_k\|^2$, for some constant μ. However, in order to have a fast convergence, a suitable initial guess should be chosen. See [47] for more details.

Since Eq. (4) exhibits a singularity at $x = 0$, we will first apply L'Hospital's rule to the second term of Eq. (4) to address the singularity at the origin [16]. We obtain

$$\nu''_{k+1}(x) + l_k(x)\nu'_{k+1}(x) + w_k(x)\nu_{k+1}(x) = h_k(x), \qquad k = 0, 1, 2, \cdots, \tag{6}$$

where

$$l_k(x) = \begin{cases} 0, & (x = 0), \\ \dfrac{\lambda}{x}, & (x \neq 0), \end{cases}, \qquad w_k(x) = \begin{cases} \dfrac{d_k(0)}{\lambda + 1}, & (x = 0), \\ d_k(x), & (x \neq 0), \end{cases}$$

and

$$h_k(x) = \begin{cases} \dfrac{b_k(0)}{\lambda + 1}, & (x = 0), \\ b_k(x), & (x \neq 0). \end{cases}$$

Now, let us rewrite Eq. (6) along with boundary conditions given in (5), in the following operator form:

$$\begin{cases} \mathbb{L}\nu_{k+1} = h_k(x), & k = 0, 1, 2, \cdots, \\ \nu'_{k+1}(0) = 0, & \gamma\nu_{k+1}(1) + \zeta\nu'_{k+1}(1) = \rho. \end{cases} \tag{7}$$

In Eq. (7), the linear operator $\mathbb{L} : \mathcal{W}^{p_{(n)}}[0, 1] \to L^2[0, 1]$ is defined as:

$$\mathbb{L}\nu_{k+1} = \nu''_{k+1}(x) + l_k(x)\nu'_{k+1}(x) + w_k(x)\nu_{k+1}(x). \tag{8}$$

Lemma 3.2. Let $w_k(x)$ be a continuous function on the interval $[0, 1]$. Then $\mathbb{L}$ is a bounded linear operator.

Proof. The proof is similar to Lemma 2.1 in [4]. □

3.1 Construction of a new basis for $\mathcal{W}^{p_{(n)}}[0, 1]$

Let $\mathbb{L}^*$ be the conjugate operator of $\mathbb{L}$, and let $\kappa(\xi, x)$ be the kernel function of $L^2[0, 1]$. Also, assume that $\{x_i\}_{i=1}^{n-1}$ are any $n - 1$ distinct nodes in $(0, 1)$. We define

$$\Phi_i(x) = \mathbb{L}^*_\xi \kappa(\xi, x)|_{\xi = x_i}, \qquad i = 1, 2, \cdots, n - 1.$$

In this equation, $\mathbb{L}^*_\xi$ means that $\mathbb{L}^*$ applies to the function of ξ. Using the properties of reproducing kernel space [4, 40], we obtain the following lemma.

Lemma 3.3. $\Phi_i(x) = \mathbb{L}_\xi \mathcal{K}(\xi, x)|_{\xi = x_i}, \quad i = 1, 2, \cdots, n - 1.$

Proof.

$$\Phi_i(x) = \langle \mathbb{L}_\xi^* \kappa(\xi,\vartheta)|_{\xi=x_i}, \mathcal{K}(\vartheta,x)\rangle_{\mathcal{W}^{p(n)}} = \langle \kappa(\xi,\vartheta), \mathbb{L}_\vartheta \mathcal{K}(\vartheta,x)|_{\vartheta=x_i}\rangle_{L^2} = \mathbb{L}_\xi \mathcal{K}(\xi,x)|_{\xi=x_i}.$$

□

Also, according to the NBCs and RBCs given in Eq. (2), we define the following two bases $\Theta_1(x)$ and $\Theta_2(x)$.

$$\Theta_1(x) = \frac{\partial}{\partial\xi}\mathcal{K}(\xi,x)|_{\xi=0}, \qquad \Theta_2(x) = \gamma\mathcal{K}(\xi,x)|_{\xi=1} + \zeta\frac{\partial}{\partial\xi}\mathcal{K}(\xi,x)|_{\xi=1}.$$

Through a process similar to Theorem 2.1 in [4], we obtain the following result.

Theorem 3.4. $\{\Phi_1(x), \Phi_2(x), \cdots, \Phi_{n-1}(x), \Theta_1(x), \Theta_2(x)\}$ are linearly independent in $\mathcal{W}^{p(n)}[0,1]$.

Since $\dim(\mathcal{W}^{p(n)}[0,1]) = n+1$, Theorem 3.4 ensures that a set $\{\Phi_1, \cdots, \Phi_{n-1}, \Theta_1, \Theta_2\}$ is the new basis of $\mathcal{W}^{p(n)}[0,1]$.

3.2 Applying the Bernoulli-RKM on Eq. (7)

In this part, we use the Bernoulli-RKM along with the spectral collocation method to solve the linear differential equations in Eq. (7). For this purpose, we use the following collocation points:

$$x_i = \frac{1}{2}\left(\cos\left(\frac{i\pi}{n}\right) + 1\right), \qquad i = 1, \cdots, n-1.$$

To solve Eq. (7), let $\nu_{n,k+1} \in \mathcal{W}^{p(n)}[0,1]$ be the approximation of ν_{k+1} in $(k+1)$-iteration. Using Theorem 3.4, $\nu_{n,k+1}$ can be presented as:

$$\nu_{n,k+1}(x) = \sum_{j=1}^{n-1} z_{j,k+1}\Phi_j(x) + s_{1,k+1}\Theta_1(x) + s_{2,k+1}\Theta_2(x), \tag{9}$$

where $z_{1,k+1}, z_{2,k+1}, \cdots, z_{n-1,k+1}, s_{1,k+1}, s_{2,k+1}$ are unknown coefficients. We find $\nu_{n,k+1}$, $(k = 0, 1, \cdots, \mathfrak{Max} - 1)$ such that:

$$\begin{cases} \mathbb{L}\nu_{n,k+1}(x_i) = h_{n,k}(x_i), \quad i = 1, \cdots, n-1, \\ \nu'_{n,k+1}(0) = 0, \qquad \gamma\nu_{n,k+1}(1) + \zeta\nu'_{n,k+1}(1) = \rho. \end{cases} \tag{10}$$

Here,

$$h_{n,k}(x) = \begin{cases} \dfrac{g(0,\nu_{n,k}) - \nu_{n,k}g_{\nu_{n,k}}(0,\nu_{n,k})}{\lambda+1}, & (x=0), \\ g(x,\nu_{n,k}) - \nu_{n,k}g_{\nu_{n,k}}(x,\nu_{n,k}), & (x\neq 0), \end{cases}$$

is a known function, and $\mathfrak{Max}$ is the maximum number of iterations.

Lemma 3.5. The linear system of equations given in Eq. (10), is equivalent to:

$$\begin{cases} \langle \nu_{n,k+1}, \Phi_i\rangle_{\mathcal{W}^{p(n)}} = h_{n,k}(x_i), \qquad i = 1, \cdots, n-1, \qquad k = 0, 1, \cdots, \mathfrak{Max} - 1, \\ \langle \nu_{n,k+1}, \Theta_1\rangle_{\mathcal{W}^{p(n)}} = 0, \\ \langle \nu_{n,k+1}, \Theta_2\rangle_{\mathcal{W}^{p(n)}} = \rho. \end{cases} \tag{11}$$

Proof. Let $\nu_{n,k+1} \in \mathcal{W}^{p(n)}[0,1]$ be the exact solution of (10). Using the properties of the reproducing kernel, we have

$$\begin{aligned}
\langle \nu_{n,k+1}, \Phi_i \rangle_{\mathcal{W}^{p(n)}} &= \big\langle \nu_{n,k+1}, \mathbb{L}_\xi^* \kappa(\xi, x)|_{\xi=x_i} \big\rangle_{\mathcal{W}^{p(n)}} = \big\langle \mathbb{L}\nu_{n,k+1}, \kappa(\xi, x)|_{\xi=x_i} \big\rangle_{L^2} \\
&= \mathbb{L}\nu_{n,k+1}(x_i) = h_{n,k}(x_i), \qquad i = 1, \cdots, n-1, \\
\langle \nu_{n,k+1}, \Theta_1 \rangle_{\mathcal{W}^{p(n)}} &= \big\langle \nu_{n,k+1}, \frac{\partial}{\partial \xi} \mathcal{K}(\xi, x)|_{\xi=0} \big\rangle_{\mathcal{W}^{p(n)}} = \frac{\partial}{\partial \xi} \big\langle \nu_{n,k+1} \mathcal{K}(\xi, x) \big\rangle|_{\xi=0} \\
&= \frac{\partial}{\partial \xi} \nu_{n,k+1}|_{\xi=0} = \nu'(0) = 0, \\
\big\langle \nu_{n,k+1}, \Theta_2 \big\rangle_{\mathcal{W}^{p(n)}} &= \Big\langle \nu_{n,k+1}, \gamma \mathcal{K}(\xi, x)|_{\xi=1} + \zeta \frac{\partial}{\partial \xi} \mathcal{K}(\xi, x)|_{\xi=1} \Big\rangle_{\mathcal{W}^{p(n)}} \\
&= \gamma \big\langle \nu_{n,k+1}, \mathcal{K}(\xi, x)|_{\xi=1} \big\rangle_{\mathcal{W}^{p(n)}} + \big\langle \nu_{n,k+1}, \zeta \frac{\partial}{\partial \xi} \mathcal{K}(\xi, x)|_{\xi=1} \big\rangle_{\mathcal{W}^{p(n)}} \\
&= \gamma \nu_{n,k+1}(1) + \zeta \frac{\partial}{\partial \xi} \big\langle \nu_{n,k+1}, \mathcal{K}(\xi, x) \big\rangle|_{\xi=1} \\
&= \gamma \nu_{n,k+1}(1) + \zeta \frac{\partial}{\partial \xi} \nu_{n,k+1}|_{\xi=1} = \rho.
\end{aligned}$$

□

Theorem 3.6. The Bernoulli-RKM (10) is uniquely solvable.

Proof. Using Lemma 3.5, by substituting (9) into the linear system (11), we obtain

$$\begin{cases}
\sum_{j=1}^{n-1} z_{j,k+1} \langle \Phi_j, \Phi_i \rangle + s_{1,k+1} \langle \Theta_1, \Phi_i \rangle + s_{2,k+1} \langle \Theta_2, \Phi_i \rangle = h_{n,k}(x_i), \quad i = 1, \cdots, n-1, \\
\sum_{j=1}^{n-1} z_{j,k+1} \langle \Phi_j, \Theta_1 \rangle + s_{1,k+1} \langle \Theta_1, \Theta_1 \rangle + s_{2,k+1} \langle \Theta_2, \Theta_1 \rangle = 0, \\
\sum_{j=1}^{n-1} z_{j,k+1} \langle \Phi_j, \Theta_2 \rangle + s_{1,k+1} \langle \Theta_1, \Theta_2 \rangle + s_{2,k+1} \langle \Theta_2, \Theta_2 \rangle = \rho.
\end{cases} \tag{12}$$

Let us define an $(n+1)$-dimensional vector $\overrightarrow{z}$ as $\overrightarrow{z}^T = [z_{1,k+1}, z_{2,k+1}, ..., z_{n-1,k+1}, s_{1,k}, s_{2,k}]$ where T indicates transposition. The matrix form of the linear system (12) may be written as:

$$\mathbf{G} \overrightarrow{z} = \overrightarrow{h}, \tag{13}$$

where

$$\mathbf{G} = \begin{bmatrix} \langle \Phi_i, \Phi_j \rangle_{(n-1)\times(n-1)} & \langle \Theta_j, \Phi_i \rangle_{(n-1)\times 2} \\ \langle \Phi_j, \Theta_i \rangle_{2\times(n-1)} & \langle \Theta_i, \Theta_j \rangle_{2\times 2} \end{bmatrix}_{(n+1)\times(n+1)}, \quad \overrightarrow{h} = \begin{bmatrix} h_{n,k}(x_1) \\ h_{n,k}(x_2) \\ \vdots \\ h_{n,k}(x_{n-1}) \\ 0 \\ \rho \end{bmatrix}. \tag{14}$$

As can be seen from Eq. (14), the coefficient matrix $\mathbf{G}$ in Eq. (13) is a Gram matrix, so $\mathbf{G}$ is symmetric and positive definite. As a result, the coefficient matrix $\mathbf{G}$ is invertible and the linear system (11) has a unique solution. □

3.3 Convergence analysis and error estimation

This part describes the convergence and error analysis of Bernoulli-RKM. Assume that $\nu(x)$ and $\nu_{k+1}(x)$ are the exact solutions of problem (1)-(2), and Eq. (7), respectively . Also, we assume that $\nu_{n,k+1}(x)$ is the approximation of $\nu_{k+1}(x)$ obtained by (10). Using triangle inequality, we get

$$\|\nu(x) - \nu_{n,k+1}(x)\| \leq \|\nu(x) - \nu_{k+1}(x)\| + \|\nu_{k+1}(x) - \nu_{n,k+1}(x)\|.$$

We have already, see Remark 3.1, talked about the first term $\|\nu(x) - \nu_{k+1}(x)\|$. It remains to obtain an upper bound for $\|\nu_{k+1}(x) - \nu_{n,k+1}(x)\|$.

Lemma 3.7. If $\mathscr{R}_{n+1}\nu_{k+1}$ denotes the orthogonal projection of ν_{k+1} on $\mathcal{W}^{p_{(n)}}[0,1]$, then $\nu_{n,k+1} = \mathscr{R}_{n+1}\nu_{k+1}$.

Proof. Similar to the proof of Lemma 3.5, we can show that $\mathscr{R}_{n+1}\nu_{k+1}$ holds in (11). The unique solvability of (11) shows that $\nu_{n,k+1} = \mathscr{R}_{n+1}\nu_{k+1}$. □

Theorem 3.8. Suppose $\nu_{k+1}(x)$ is sufficiently smooth. Then

$$\|\nu_{k+1}(x) - \nu_{n,k+1}(x)\| \leq \frac{1}{2^{2n+1}(n+1)!} \max_{x\in[0,1]} |\nu_{k+1}^{(n+1)}(x)|. \tag{15}$$

Proof. Using Lemma 3.7, we can conclude that

$$\langle \nu_{k+1} - \underbrace{\mathscr{R}_{n+1}\nu_{n,k+1}}_{\nu_{n,k+1}}, \omega_n \rangle = 0, \qquad \forall \omega_n \in \mathcal{W}^{p_{(n)}}[0,1]. \tag{16}$$

We have from (16) that (see say [49])

$$\|\nu_{k+1} - \nu_{n,k+1}\| \leq \inf_{\omega_n \in \mathcal{W}^{p_{(n)}}[0,1]} \|\nu_{k+1} - \omega_n\|.$$

Let $q_n(x) \in \mathcal{W}^{p_{(n)}}[0,1]$ be the interpolation polynomial which interpolates $\nu_{k+1}(x)$ at distinct points $\{\widehat{x}_i\}_{i=1}^{n+1}$ in $[0,1]$ (i.e., $q_n(\widehat{x}_i) = \nu_{k+1}(\widehat{x}_i)$). If we choose Chebyshev nodes on $[0,1]$ as:

$$\widehat{x}_i = \frac{1}{2} + \frac{1}{2}\cos\left(\frac{(2i-1)\pi}{2n+2}\right), \quad i = 1, ..., n+1,$$

then the interpolation error is given by

$$|\nu_{k+1}(x) - q_n(x)| \leq \frac{1}{2^{2n+1}(n+1)!} \max_{x\in[0,1]} |\nu_{k+1}^{(n+1)}(x)|. \tag{17}$$

This completes the proof. □

4 Numerical experiments

This section contains six illustrations that demonstrate the effectiveness and accuracy of our approach. The Examples 4.1-4.5 directly correspond to Eq. (1) with nonlinear source functions of types (i), (ii), (iii), (iv), and (v). Furthermore, Example 4.6 represents a derivative-dependent doubly SBVP as detailed in [20]. For problems for which the exact solution is known, we evaluate the accuracy of the method by reporting the following maximum absolute error:

$$MAE_{n,\mathfrak{Max}} = \max_{x\in[0,1]} |\nu(x) - \nu_{n,\mathfrak{Max}}(x)|,$$

where, $\nu(x)$ represents the exact solution, and $\nu_{n,\mathfrak{Max}}(x)$ is an approximate solution obtained from (10) using $n-1$ collocation points. Also, for problems where we don't know the exact solution, we assess the efficiency and accuracy of the Bernoulli-RKM by reporting the absolute residual error function $ER_{n,\mathfrak{Max}}(x)$ and the maximum absolute residual error $MER_{n,\mathfrak{Max}}$, which are defined respectively as:

$$ER_{n,\mathfrak{Max}}(x) = \left|\mathbb{L}\nu_{n,\mathfrak{Max}}(x) - h_{n,\mathfrak{Max}-1}(x)\right|,$$

and

$$MER_{n,\mathfrak{Max}} = \max_{x\in[0,1]}(ER_{n,\mathfrak{Max}}(x)).$$

Moreover, as mentioned in Remark 3.1, it is necessary to obtain a good initial guess for the QLM. It is usually advantageous for $\nu_0(x)$ to satisfy the boundary conditions. In this paper, for Examples 4.1, 4.2, 4.4, and 4.5, according to the NBCs and RBCs given in Eq. (2), the initial guess is taken as:

$$\nu_0(x) = -\frac{0.01(\gamma+2\zeta)-\rho}{\gamma} + 0.01x^2, \quad \gamma \neq 0. \tag{18}$$

We performed our computations using Maple 17 on a personal computer equipped with Core i5 processor and 6 GB of memory.

Example 4.1. ([5, 6, 14, 18]). We consider Eq. (1) with a non-linear source function of type (i), where $\sigma = 0.76129$, $\varrho = 0.03119$. Also, the values of the constants in (2) are $\zeta = 1$, and $\gamma = \rho = 5$. There is no analytical solution to this example. In Table 1, the results of the presented method with $\mathfrak{Max} = 2$ and $n = 10$ are compared with the domain decomposition optimal homotopy analysis method (DDOHAM) [18], the improved differential transform method (IDTM) [14], the advanced Adomian decomposition method (AADM) [6], and the SRKM [5]. The comparison presented in Table 1, shows that these methods agree well with each other. Also, we compare our method with SRKM [5] in terms of $MER_{n,1}$ as shown in Table 2. Additionally, this table includes the CPU time (s) for our method. Table 2 illustrates that Bernoulli-RKM exhibits higher accuracy than SRKM, and it is noteworthy that the computational time of the current method is very low. Moreover, absolute residual error functions with $n = 14, 15$, and $\mathfrak{Max} = 1$ are plotted in Figure 1.

Example 4.2. ([4, 5, 9, 10, 14, 18]). In this example, we consider Eq. (1) with a non-linear source function of type (ii), where $\sigma = 1$ and $\rho = 0$. We report the results for the following four cases:

Case 1: $\mu = \gamma = \zeta = 1$,

Case 2: $\mu = 1$, $\gamma = 2$ and $\zeta = 1$,

Case 3: $\mu = 1$, $\gamma = 0.1$ and $\zeta = 1$.

Case 4: $\mu = 10$, $\gamma = 4$ and $\zeta = 1$.

We do not have any analytic solution to this example. For **Case** 1, in Table 3, the numerical results of the Bernoulli-RKM with $\mathfrak{Max} = 3$, and $n = 10$ are compared with the DDOHAM [18], the IDTM [14], the SRKM [5], and the Sinc-Galerkin method (SGM) [9]. Also, Table 4 shows the comparison of the absolute residual error function of the Bernoulli-RKM with $\mathfrak{Max} = 1$ and the SRKM [4] for **Case** 2. Table 4 shows that Bernoulli-RKM has much better accuracy compared to SRKM, and the accuracy of this method increases as the number of basis functions increases.

x	DDOHAM [18] $N=5,\ n=4$	IDTM [14] $n=12$	AADM [6] $n=12$	SRKM [5] $n=10,\ k=4$	Present method $n=10$
0.0	0.8284830967	0.8284832870	0.8284832870	0.8284833754	0.8284832903
0.1	0.8297058988	0.8297060890	0.8297060890	0.8297061155	0.8297060924
0.2	0.8333745399	0.8333747303	0.8333747302	0.8333747353	0.8333747336
0.3	0.8395089283	0.8394899106	0.8394899106	0.8394899068	0.8394899139
0.4	0.8480654950	0.8480527816	0.8480527816	0.8480527759	0.8480527850
0.5	0.8591864005	0.8590649239	0.8590649238	0.8590649167	0.8590649271
0.6	0.8726159876	0.8725283166	0.8725283166	0.8725283100	0.8725283199
0.7	0.8887789925	0.8884453023	0.8884453022	0.8884452975	0.8884453056
0.8	0.9070573450	0.9068185448	0.9068185447	0.9068185422	0.9068185480
0.9	0.9282044565	0.9276509853	0.9276509852	0.9276509849	0.9276509883
1.0	0.9513015634	0.9509457960	0.9509457960	0.9509457969	0.9509457984

Table 1: Comparison of the numerical results for Example 4.1.

n	SRKM [5] $k=4$	Present method $\mathfrak{Max}=1$	CPU time
4	4.25E-05	7.60E-6	0.531
6	6.14E-06	1.35E-8	0.578
8	1.38E-06	1.74E-11	0.594
10	8.39E-07	1.89E-14	0.625

Table 2: Comparison of the maximum absolute residual error for Example 4.1.

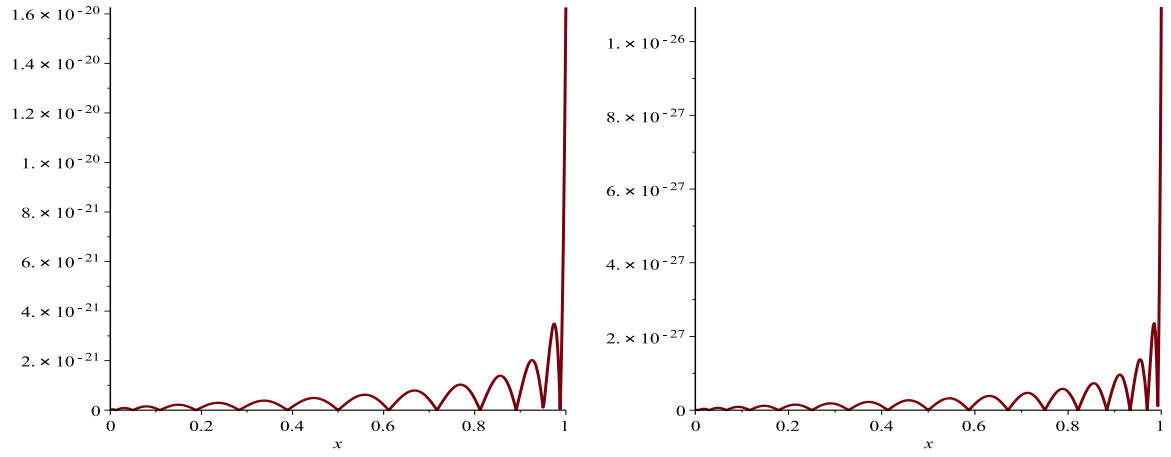

Figure 1: Graph of $ER_{n,1}(x)$, with $n = 14$ (left) and $n = 18$ (right), for Example 4.1.

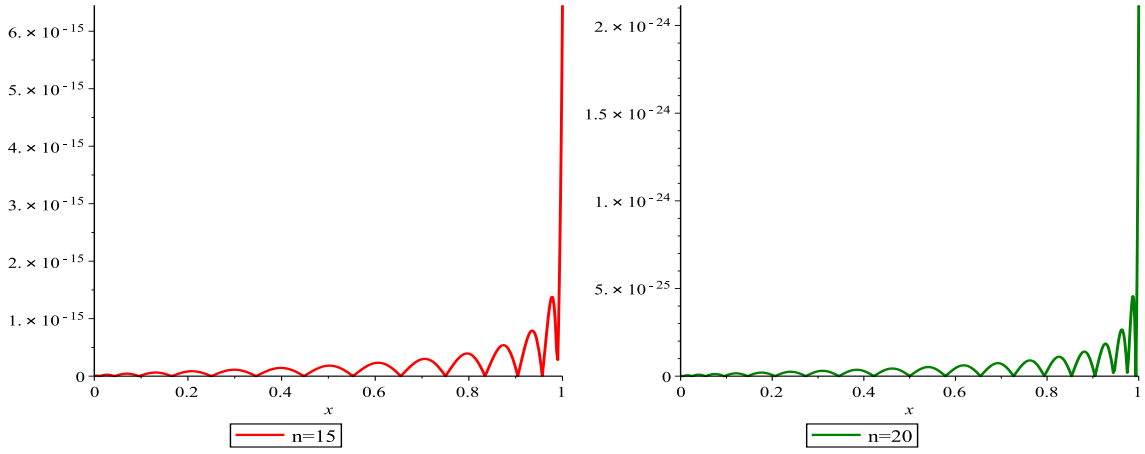

Figure 2: Graph of $ER_{n,3}(x)$ for **Case** 1 (left) and **Case** 3 (right), for Example 4.2.

Additionally, the $ER_{n,3}(x)$ for both **Cases** 1 and 3 are illustrated in Figure 2. For **Case** 4, in Table 5, the maximum absolute residual error and the CPU time of the Bernoulli-RKM with $\mathfrak{Max} = 1$, and different values of $n = 4, 6, 8, 10$ are compared with the results obtained by a method based on a modified homotopy analysis method [10]. Table 5 shows that the current method has significantly higher accuracy than the method presented in [10]. Additionally, it demonstrates that the computational time of the current method is very low. We also plot the logarithmic graph of $MER_{n,3}$, $(\log_{10}(MER_{n,3}))$ of Bernoulli-RKM with different values of $n = 4, 8, 12, 16, 20$ for **Case** 1, **Case** 2, **Case** 3 and **Case** 4 in Figure 3. From Figure 3, we can see that the $\log_{10}(MER_{n,3})$ decreases rapidly as n increases.

Example 4.3. ([22]). Let us consider Eq. (1) with a non-linear source function of type (iii) where $\lambda = 1$, and $\theta = 1$. Also, the values of the constants in (2) are $\gamma = 0$, $\zeta = 1$, and $\rho = 4/7$. The exact solution is:

$$\nu(x) = \ln\left(\frac{64}{x^4 - 16x^2 + 64}\right).$$

x	DDOHAM [18] $N=5,\ n=4$	IDTM [14] $n=12$	SRKM [5] $n=10,\ k=3$	SGM [9] $M=40$	Present method $n=10$
0.0	0.3675135205	0.3675167997	0.3675166189	0.3675168124	0.3675168150
0.1	0.3663590308	0.3663623137	0.3663622527	0.3663623265	0.3663623291
0.2	0.3628907562	0.3628940507	0.3628940189	0.3628940634	0.3628940660
0.3	0.3571336159	0.3570975301	0.3570975087	0.3570975430	0.3570975456
0.4	0.3489737609	0.3489484049	0.3489483815	0.3489484178	0.3489484205
0.5	0.3387004028	0.3384121330	0.3384121172	0.3384121459	0.3384121486
0.6	0.3256760709	0.3254435063	0.3254434945	0.3254435196	0.3254435223
0.7	0.3110427573	0.3099860240	0.3099860196	0.3099860373	0.3099860401
0.8	0.2928786338	0.2919710864	0.2919711009	0.2919711001	0.2919711029
0.9	0.2742437526	0.2713169936	0.2713170010	0.2713170072	0.2713170101
1.0	0.2505516417	0.2479277073	0.2479277424	0.2479277203	0.2479277232

Table 3: Comparison of the numerical results for Example 4.2 (**Case** 1).

	SRKM [4]		Present method	
x	$n=8$	$n=10$	$n=8$	$n=10$
0.2	9.17614E-06	5.59474E-06	7.65385E-13	2.91047E-15
0.4	4.37089E-07	7.15070E-07	1.58178E-12	2.96101E-14
0.6	4.37001E-07	1.37600E-06	2.73729E-12	4.62095E-14
0.8	1.50857E-05	6.88321E-06	4.69236E-12	1.31123E-14
1.0	6.19418E-05	2.53189E-05	4.79590E-11	8.98164E-13

Table 4: Comparison of the absolute residual error function, for Example 4.2 (**Case** 2).

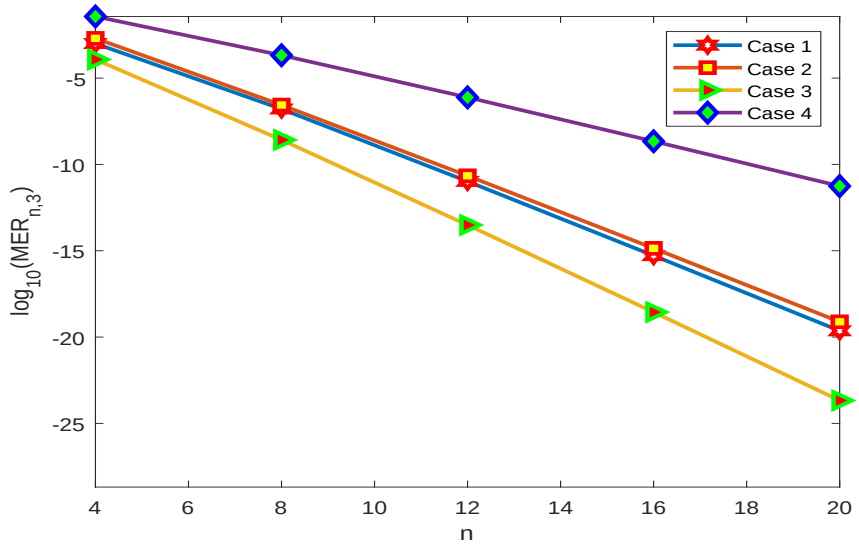

Figure 3: Graph of $\log_{10}(MER_{n,3})$ for different values of $n = 4, 8, 12, 16, 20$, for Example 4.2.

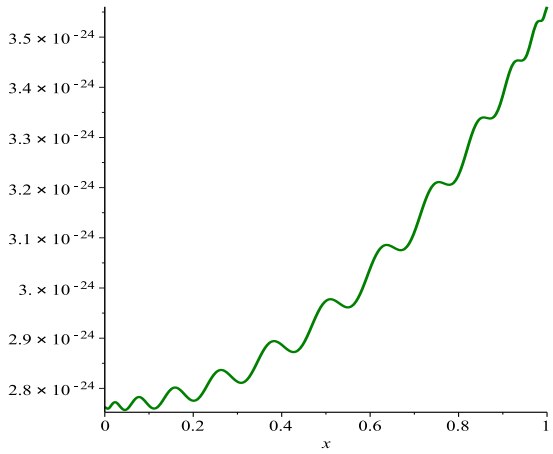

Figure 4: Graph of absolute error function $|\nu(x) - \nu_{n,4}(x)|$ with $n = 25$, for Example 4.3.

In this example, we put $\nu_0(x) = 0.01 + 2/7\ x^2$. It can be seen that $\nu_0(x)$ satisfies the boundary conditions in Eq. (2). The absolute error function $|\nu(x) - \nu_{n,4}(x)|$ is plotted in Figure 4. Also, Table 6 shows the obtained values of $MAE_{n,4}$ for $n = 5, 10, 15, 20$ and CPU time in seconds. It is obvious from Table 6 that with the increase of n, the maximum absolute error decreases rapidly. Also, in Table 6, we can see that the computational time of the current method is significantly low.

n	4	6	8	10
$MER_{n,1}$				
Method of [10]	0.0758	0.0307	0.0131	0.0057
Bernoulli-RKM	3.50E-02	6.30E-04	1.10E-06	3.22E-08
CPU time				
Method of [10]	1.40	3.28	8.53	
Bernoulli-RKM	0.578	0.578	0.610	0.828

Table 5: Comparison of the maximum absolute residual error and the CPU time in seconds for Example 4.2 (**Case** 4).

n	5	10	15	20
$MAE_{n,4}$	8.80E-05	1.08E-09	1.60E-14	2.37E-19
CPU time	0.609	0.985	2.000	4.328

Table 6: The values of $MAE_{n,4}$ and CPU time in seconds for Example 4.3.

Example 4.4. ([9, 50, 51]). Consider Eq. (1) with a non-linear source function of type (iv) where $\lambda = 2$, $\gamma = 1$, $\zeta = 0$, and $\rho = 1$. This example represents the reaction-diffusion process in a porous spherical catalyst (e.g., see [9, 50] and references therein). In this example, the values of two parameters φ (utilized to describe a dimensionless group called the Thiele modulus) and η (effectiveness factor) are very important. For a spherical catalyst pellet, η is defined as [9]:

$$\eta = \frac{3}{\varphi^2}\frac{d\nu}{dx}\bigg|_{x=1}. \tag{19}$$

To make a comparison, in Table 7, we compare the results for effectiveness factor η of Bernoulli-RKM with $\mathfrak{Max} = 4$ together with the results obtained by SGM [9], optimal homotopy analysis method (OHAM) [50], and the numerical solution obtained by shooting method [51] for different values of φ and m. Also, in Table 8, the numerical results of the Bernoulli-RKM with $\mathfrak{Max} = 4, \varphi = 5$, and $m = 1.5$ are compared with the SGM [9] and the shooting method [51]. We observe from Tables 7 and 8, that our numerical results are in excellent agreement with the numerical results given in [51]. Furthermore, to show the efficiency of the Bernoulli-RKM, the absolute residual error function $ER_{15,1}(x)$ is plotted in Figure 5. We end this example by plotting a logarithmic graph of $MER_{n,1}$, $(\log_{10}(MER_{n,1}))$ for Bernoulli-RKM. We use different values of $n = 7, 11, 15, 19, 23$ with $\varphi = 5$, $m = 1.5$ and $\varphi = 5$, $m = 1$ in Figure 6. This figure illustrates that the distribution of points is nearly linear, indicating the rapid convergence of an exponential rate.

m	φ	Method		$n=9$	$n=14$
		Numerical [51]	0.879262		
		SGM [9]	0.879260		
		OHAM [50]	0.879249		
0.5	2	Bernoulli-RKM		0.879261	0.879262
		Numerical [51]	0.480054		
		SGM [9]	0.480040		
		OHAM [50]	0.480056		
1	5	Bernoulli-RKM		0.480053	0.480054
		Numerical [51]	0.431958		
		SGM [9]	0.431941		
		OHAM [50]	0.432001		
1.5	5	Bernoulli-RKM		0.431926	0.431958
		Numerical [51]	0.397233		
		SGM [9]	0.397214		
		OHAM [50]	0.397192		
2	5	Bernoulli-RKM		0.397124	0.397233

Table 7: Comparison of the values of η, for Example 4.4.

x	Numerical [51]	SGM [9] $M = 10$	Bernoulli-RKM $n = 11$
0.0	0.177518	0.177518	0.177518
0.1	0.180659	0.180659	0.180659
0.2	0.190386	0.190383	0.190386
0.3	0.207669	0.207663	0.207669
0.4	0.234322	0.234338	0.234322
0.5	0.273373	0.273373	0.273373
0.6	0.329732	0.329715	0.329732
0.7	0.411406	0.411414	0.411406
0.8	0.531770	0.531774	0.531769
0.9	0.713974	0.713974	0.713974
1.0	1.000000	1.000000	1.000000

Table 8: Comparison of $\nu(x)$ for $\varphi = 5,\ m = 1.5$, for Example 4.4.

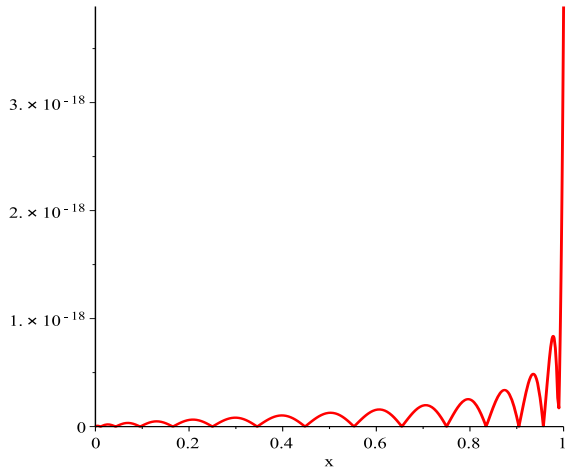

Figure 5: Graph of $ER_{15,1}(x)$ with $\varphi = 2$, and $m = 0.5$, for Example 4.4.

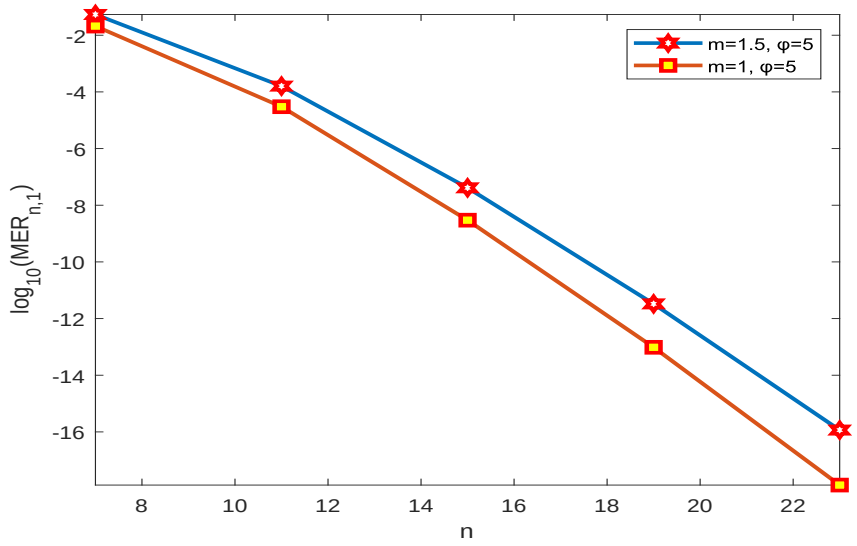

Figure 6: Graph of $\log_{10}(MER_{n,1})$ for different values of $n = 7, 11, 15, 19, 23$, for Example 4.4.

Example 4.5. ([17]). Consider Eq. (1) with a non-linear source function of type (v) where $\lambda = 2$, $\gamma = 1$, $\zeta = 0$, and $\rho = \sqrt{\frac{3}{4}}$. The exact solution is:

$$\nu(x) = \sqrt{\frac{3}{x^2 + 3}}.$$

The absolute error function $|\nu(x) - \nu_{n,4}(x)|$ is plotted in Figure 7. We also plot the logarithmic graph of $MAE_{n,5}$, $(\log_{10}(MAE_{n,5}))$ of the presented method with $n = 4, 8, 12, 16, 20$ in Figure 8. Moreover, in Table 9, we compare the maximum absolute errors of our method for $n = 4, 6, 8$ and $\mathfrak{Max} = 4$ with the results from the fourth order domain decomposition homotopy perturbation method (DDHPM) presented in [17]. Additionally, this table includes the CPU time in seconds for the presented method.

	DDHPM [17]	Bernoulli-RKM	
n	$(N = 4)$	$(\mathfrak{Max} = 4)$	CPU time
4		2.4000E-04	0.578
6	5.4263E-05	2.2000E-06	0.657
8	3.7898E-06	1.8155E-08	0.766

Table 9: Comparison of the maximum absolute error for Example 4.5.

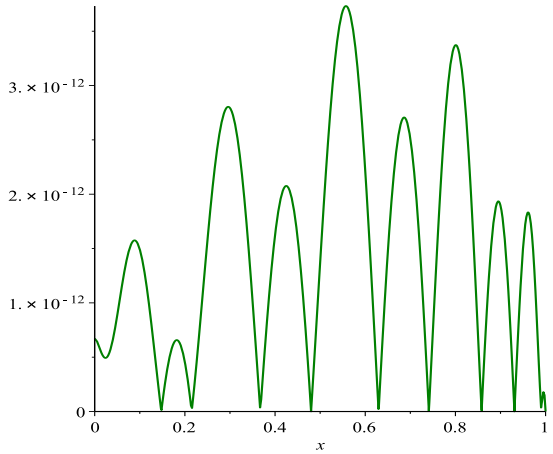

Figure 7: Graph of absolute error function $|\nu(x) - \nu_{n,4}(x)|$ with $n = 12$, for Example 4.5.

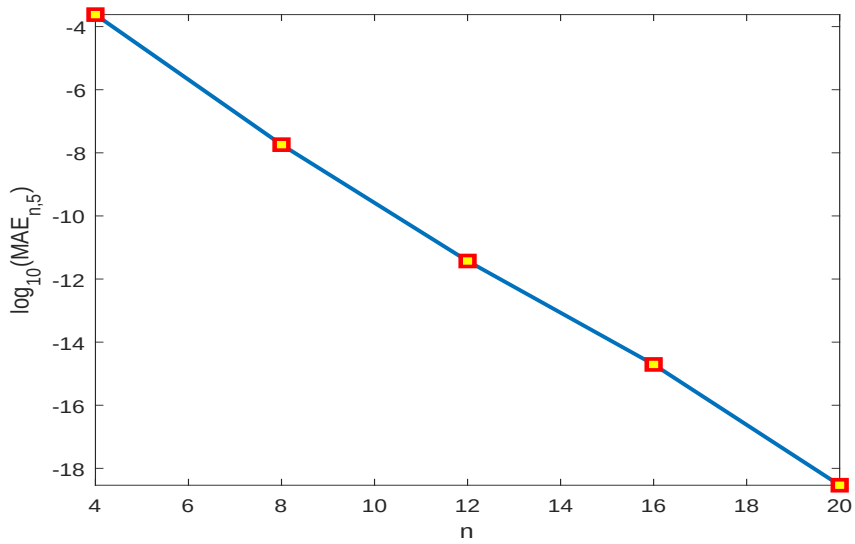

Figure 8: Graph of $\log_{10}(MAE_{n,5})$ for different values of $n = 4, 8, 12, 16, 20$, for Example 4.5.

Example 4.6. ([20]). As our last example, we consider a linear derivative dependent doubly singular boundary value problems as follows:

$$\left(x^{\alpha}\nu'(x)\right)' = \beta x^{\alpha+\beta-2}\left(x\nu'(x) + (\alpha+\beta-1)\,\nu(x)\right),$$

$$\nu(0) = 1, \qquad \nu(1) = exp(1).$$

The exact solution of this example is $\nu(x) = exp(x^{\beta})$. We solve this problem for $\alpha = 0.25$ and $\beta = 1$. Since this example is a linear problem, there is no need to use the quasi-linearization method. It can be easily solved with an approach similar to the method presented in Section 3. In Figure 9, the logarithmic graph of the maximum absolute errors, denoted as $(\log_{10}(MAE_n))$, for

our method is plotted for different values of n. This graph clearly demonstrates a rapid decrease in the maximum absolute errors as the value of n increases. Also, in Table 10, we compare the maximum absolute errors obtained for $n = 6, 10, 14$ with the results of the improved homotopy analysis method (IHAM) presented in [20]. Additionally, this table provides the CPU time in seconds for our approach. As observed in Table 10, our proposed method demonstrates better accuracy compared to IHAM [20]. It is important to note that the computational time of our method is significantly low.

	IHAM [20]	Bernoulli-RKM	
n	$(\alpha = 0.25,\ \beta = 1)$	$(\alpha = 0.25,\ \beta = 1)$	CPU time
6	5.5742E-07	9.6997E-08	0.281
10	3.2807E-10	4.5068E-14	0.407
14		5.1975E-21	0.453

Table 10: Comparison of the maximum absolute error for Example 4.6.

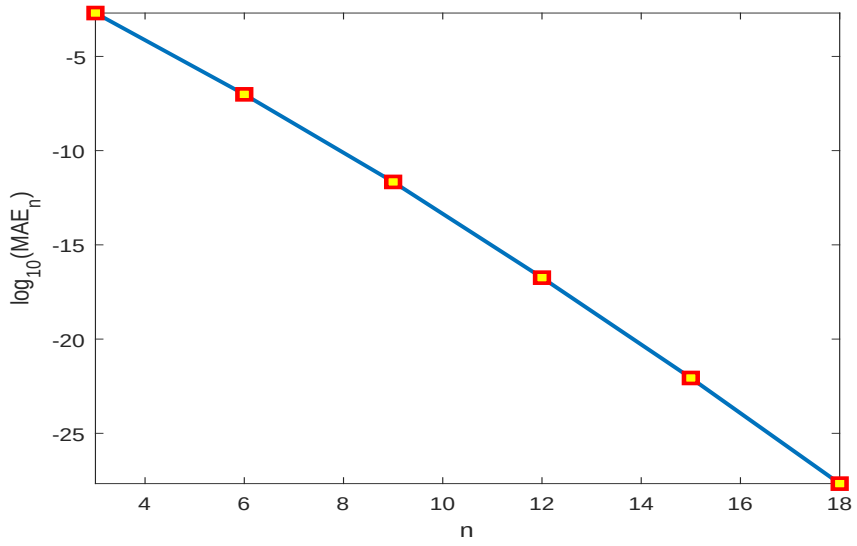

Figure 9: Graph of $\log_{10}(MAE_n)$ for different values of n for Example 4.6.

5 Conclusion

In the current study, a new Bernoulli-RKM is introduced and successfully applied to solve a class of SBVPs with Neumann and Robin boundary conditions. To construct this method, orthonormal Bernoulli polynomials, quasi-linearization techniques, and classical RKM ideas play a fundamental role. Also, we proved the solvability of a set of linear algebraic equations that appears in Bernoulli-RKM, and the convergence of our method.

The method described in this article deals with some of the limitations of classical RKM. Bernoulli-RKM eliminates the reliance on the Gram-Schmidt orthogonalization process and the necessity to choose a dense set of points. As a result, Bernoulli-RKM achieves highly accurate numerical results using far fewer nodes compared to classical RKM and some other semi-analytical and numerical methods. Indeed, our method effectively reduces CPU time by eliminating the Gram-Schmidt orthogonalization process.

Moreover, Bernoulli-RKM applies to six examples, and our numerical findings are compared with exact solutions, as well as existing results. From a computational point of view, the solutions obtained using Bernoulli-RKM are in excellent agreement with the results of previous studies. Furthermore, the logarithmic plots of the errors, as depicted in Figures 3, 6, 8, and 9, exhibit a nearly linear distribution of points. This observation suggests the convergence at an exponential rate.

Acknowledgments: We express our sincere thanks to the anonymous referees for valuable suggestions that improved the final manuscript.

References

[1] J. Guo, A. Khan, M. Sulaiman, P. Kumam, A novel neuroevolutionary naradigm for solving strongly nonlinear singular boundary value vroblems in physiology, IEEE Access, 10 (2022) 21979-22002.

[2] B. F. Gray, The distribution of heat sources in the human head-theoretical consideration, Journal of Theoretical Biology, 82 (1980) 473-476.

[3] S. H. Lin, Oxygen diffusion in a spherical cell with nonlinear oxygen uptake kinetics, Journal of Theoretical Biology, 60 (1976) 449-457.

[4] J. Niu, M. Xu, Y. Lin, Q. Xue, Numerical solution of nonlinear singular boundary value problems, Journal of Computational and Applied Mathematics, 331 (2018) 42-51.

[5] H. Zhu, J. Niu, R. Zhang, Y. Lin, A new approach for solving nonlinear singular boundary value problems, Mathematical Modelling and Analysis, 23 (2018) 33-43.

[6] Umesh, M. Kumar, Numerical solution of singular boundary value problems using advanced Adomian decomposition method, Engineering with Computers, 37 (2021) 2853-2863.

[7] R. K. Pandey, A. K. Verma, Existence-uniqueness results for a class of singular boundary value problems arising in physiology, Nonlinear Analysis: Real World Applications 9 (2008) 40-52.

[8] S. H Chang, Electroosmotic flow in a dissimilarly charged slit microchannel containing salt-free solution, European Journal of Mechanics-B/Fluids, 34 (2012) 85-90.

[9] E. Babolian, A. Eftekhari, A. Saadatmandi, A Sinc-Galerkin technique for the numerical solution of a class of singular boundary value problems, Computational and Applied Mathematics, 34 (2015) 45-63.

[10] P. Roul, A fast and accurate computational technique for efficient numerical solution of nonlinear singular boundary value problems, International Journal of Computer Mathematics, 96 (2019) 51-72.

[11] M. Xu, E. Tohidi, A Legendre reproducing kernel method with higher convergence order for a class of singular two-point boundary value problems, Journal of Applied Mathematics and Computing, 67 (2021) 405-421.

[12] R. Singh, J. Kumar, An efficient numerical technique for the solution of nonlinear singular boundary value problems, Computer Physics Communications, 185 (2014) 1282-1289.

[13] S. H. Chang, A variational iteration method involving Adomian polynomials for a strongly nonlinear boundary value problem, East Asian Journal on Applied Mathematics, 9 (2019) 153-164.

[14] L. J. Xie, C. L. Zhou, S. Xu, An effective numerical method to solve a class of nonlinear singular boundary value problems using improved differential transform method, SpringerPlus, 5 (2016) 1-19.

[15] M. Mohsenyzadeh, K. Maleknejad, R. Ezzati, A numerical approach for the solution of a class of singular boundary value problems arising in physiology, Advances in Difference Equations, 2015 (2015) 1-10.

[16] A. R. Kanth, V. Bhattacharya, Cubic spline for a class of non-linear singular boundary value problems arising in physiology, Applied Mathematics and Computation, 174 (2006) 768-774.

[17] P. Roul, On the numerical solution of singular two-point boundary value problems: A domain decomposition homotopy perturbation approach, Mathematical Methods in the Applied Sciences, 40 (2017) 7396-7409.

[18] P. Roul, H. Madduri, A new highly accurate domain decomposition optimal homotopy analysis method and its convergence for singular boundary value problems, Mathematical Methods in the Applied Sciences, 41 (2018) 6625-6644.

[19] P. Roul, H. Madduri, K. Kassner, A new iterative algorithm for a strongly nonlinear singular boundary value problem, Journal of Computational and Applied Mathematics, 351 (2019) 167-178.

[20] P. Roul, Doubly singular boundary value problems with derivative dependent source function: A fast-converging iterative approach, Mathematical Methods in the Applied Sciences, 42 (2019) 354-374.

[21] P. Roul, A new mixed MADM-collocation approach for solving a class of Lane-Emden singular boundary value problems, Journal of Mathematical Chemistry, 57 (2019) 945-969.

[22] C. S. Liu, E. R. El-Zahar, C. W. Chang, A boundary shape function iterative method for solving nonlinear singular boundary value problems, Mathematics and Computers in Simulation, 187 (2021) 614-629.

[23] P. Roul, V. P. Goura, Numerical solution of doubly singular boundary value problems by finite difference method, Computational and Applied Mathematics, 39 (2020) 1-25.

[24] A. Eftekhari, Spectral poly-sinc collocation method for solving a singular nonlinear BVP of reaction-diffusion with Michaelis-Menten kinetics in a catalyst/biocatalyst, Iranian Journal of Mathematical Chemistry, 14 (2023) 77-96.

[25] A. Saadatmandi, N. Nafar, S. P. Toufighi, Numerical study on the reaction cum diffusion process in a spherical biocatalyst, Iranian Journal of Mathematical Chemistry, 5 (2014) 47-61.

[26] P. Roul, V. P. Goura, R. Agarwal, A compact finite difference method for a general class of nonlinear singular boundary value problems with Neumann and Robin boundary conditions, Applied Mathematics and Computation, 350 (2019) 283-304.

[27] Y. H. Youssri, S. M. Sayed, A. S. Mohamed, E. M. Aboeldahab, W. M. Abd-Elhameed, Modified Lucas polynomials for the numerical treatment of second-order boundary value problems, Computational Methods for Differential Equations, 11 (2023) 12-31.

[28] A. Eftekhari, A. Saadatmandi, DE Sinc-collocation method for solving a class of second-order nonlinear BVPs, Mathematics Interdisciplinary Research 6 (2021) 11-22.

[29] P. Roul, H. Madduri, K. Kassner, A sixth-order numerical method for a strongly nonlinear singular boundary value problem governing electrohydrodynamic flow in a circular cylindrical conduit, Applied Mathematics and Computation, 350 (2019) 416-433.

[30] P. Roul, K. Thula, R. Agarwal, Non-optimal fourth-order and optimal sixth-order B-spline collocation methods for Lane-Emden boundary value problems, Applied Numerical Mathematics, 145 (2019) 342-360.

[31] P. Roul, A fourth-order non-uniform mesh optimal B-spline collocation method for solving a strongly nonlinear singular boundary value problem describing electrohydrodynamic flow of a fluid, Applied Numerical Mathematics, 153 (2020) 558-574.

[32] M. Bagherzadeh, A. Neamaty, The Borg's theorem for singular Sturm-Liouville problem with non-separated boundary conditions, Mathematics Interdisciplinary Research 8 (2023) 233-245.

[33] R. K. Pandey, S. Tomar, An effective scheme for solving a class of nonlinear doubly singular boundary value problems through quasilinearization approach, Journal of Computational and Applied mathematics, 392 (2021) 113411.

[34] M. Lakestani, M. Dehghan, Four techniques based on the B-spline expansion and the collocation approach for the numerical solution of the Lane-Emden equation, Mathematical Methods in the Applied Sciences, 36 (2013) 2243-2253.

[35] M. Dehghan, F. Shakeri, Approximate solution of a differential equation arising in astrophysics using the variational iteration method, New Astronomy, 13 (2008) 53-59.

[36] M. Dehghan, A. Nikpour, Numerical solution of the system of second-order boundary value problems using the local radial basis functions based differential quadrature collocation method, Applied Mathematical Modelling, 37 (2013) 8578-8599.

[37] M. Dehghan, F. Shakeri, A semi-numerical technique for solving the multi-point boundary value problems and engineering applications, International Journal of Numerical Methods for Heat and Fluid Flow, 21 (2011) 794-809.

[38] M. Dehghan, M. Tatari, Finding approximate solutions for a class of third-order non-linear boundary value problems via the decomposition method of Adomian, International Journal of Computer Mathematics, 87 (2010) 1256-1263.

[39] S. Zaremba, Sur le calcul numérique des fonctions demandées dans le probléme de Dirichlet et le probléme hydrodynamique, Imprimerie de l'Universite, (1909) 125-195.

[40] M. Cui, Y. Lin, Nonlinear numerical analysis in the reproducing kernel space, Nova Science Publishers, Inc, 2009.

[41] Z. Chen, W. Jiang, H. Du, A new reproducing kernel method for Duffing equations, International Journal of Computer Mathematics, 98 (2021) 2341-2354.

[42] M. G. Sakar, O. Saldlr, A. Akgül, Numerical solution of fractional Bratu type equations with Legendre reproducing kernel method, International Journal of Applied and Computational Mathematics, 4 (2018) 126.

[43] S. Farzaneh Javan, S. Abbasbandy, M. A. Fariborzi Araghi, Application of reproducing kernel Hilbert space method for solving a class of nonlinear integral equations, Mathematical Problems in Engineering, 2017 (2017), article ID 7498136.

[44] S. Mashayekhi, Y. Ordokhani, M. Razzaghi, Hybrid functions approach for optimal control of systems described by integro-differential equations, Applied Mathematical Modelling, 37 (2013) 3355-3368.

[45] F. Mirzaee, N. Samadyar, Explicit representation of orthonormal Bernoulli polynomials and its application for solving Volterra-Fredholm-Hammerstein integral equations, SeMA Journal, 77 (2020) 81-96.

[46] F. Deutsch , Best Approximation in Inner Product Spaces, Springer, New York, 2001.

[47] V. B. Mandelzweig, F. Tabakin, Quasilinearization approach to nonlinear problems in physics with application to nonlinear ODEs, Computer Physics Communications, 141 (2001) 268-281.

[48] K. Parand, A. Ghaderi-Kangavari, M. Delkosh, Two efficient computational algorithms to solve the nonlinear singular Lane-Emden equations, Astrophysics, 63 (2020) 133-150.

[49] J. Shen, T. Tang, L. Wang, Spectral methods: algorithms, analysis and applications, Springer, 2011.

[50] M. Danish, S. Kumar, S. Kumar, A note on the solution of singular boundary value problems arising in engineering and applied sciences: use of OHAM. Computers and chemical engineering, 36 (2012) 57-67.

[51] D. B. Meade, B. S. Haran, R. E. White, The shooting technique for the solution of two-point boundary value problems, Maple Technical Newsletter, 3 (1996) 1-8.